

# Supporting Online Material for

# **Identification of a Primary Target of Thalidomide Teratogenicity**

Takumi Ito, Hideki Ando, Takayuki Suzuki, Toshihiko Ogura, Kentaro Hotta, Yoshimasa Imamura, Yuki Yamaguchi, Hiroshi Handa\*

\*To whom correspondence should be addressed. E-mail: handa.h.aa@m.titech.ac.jp

Published 12 March 2010, *Science* **327**, 1345 (2010) DOI: 10.1126/science.1177319

### This PDF file includes

Materials and Methods SOM Text Figs. S1 to S19 Tables S1 and S2 References

# **Supporting Online Material**

### MATERIALS AND METHODS

**Reagents.** For cell culture experiments, thalidomide (Tocris Cookson) was dissolved in dimethylsulfoxide (DMSO) at room temperature to make up 100 mM stock solution. For zebrafish experiments, thalidomide was dissolved in DMSO to make up 400 mM stock solution, which was done by repeating the following steps more than ten times: heating for 2 min at 65°C and vigorous shaking for 2 min at room temperature. The higher concentration stock was required to keep the final concentration of DMSO under 0.1%.

**Preparation of thalidomide-immobilized beads.** Scheme of immobilization is shown in fig. S1. Magnetic FG beads (5 mg) (*S1*), were incubated with 10 mM 1-hydroxybenzotriazole, 10 mM 1-ethyl-3-(3-demithyl- aminopropyl)-carbodiimide HCl, and 2 mM carboxyl thalidomide derivative FR259625 in *N*,*N*-dimethylformamide for 4 h at room temperature. Unreacted residues were masked using 20% carbonic anhydride in *N*,*N*-dimethylformamide, and the resulting beads were stored at 4°C.

### Affinity purification with thalidomide-immobilized beads.

Thalidomide-immobilized beads (0.5 mg) were equilibrated with 0.5% NP-40 lysis buffer containing 50 mM Tris-HCl (pH 8.0), 150 mM NaCl, and 0.5% NP-40. Cell extracts (10 mg) were prepared from human HeLa, Jurkat, THP-1, U266, HUVEC, LP101, SH-SY5Y, and 293T cells and mouse N1E-115 cells as described and were incubated with the beads for 2 h at 4°C (S2). The beads were washed three times with 0.5% NP-40 lysis buffer, and bound proteins were eluted with the same buffer containing 1 mM thalidomide. In some experiments, 0.3 mM thalidomide was added to extracts before incubation with the beads.

**Plasmids.** Human CRBN and DDB2 cDNAs were obtained by RT-PCR from HeLa total RNA. A series of CRBN mutants were generated by standard PCR techniques. DDB1 cDNA was provided by T. Matsunaga (Kanazawa Univ., Kanazawa, Japan). *zcrbn* and *zcul4a* cDNAs were obtained by RT-PCR from 24-hpf zebrafish total RNA. Mouse CRBN (mCRBN) cDNA was obtained by RT-PCR from mouse bEnd3 total RNA. Chick *crbn* (*ccrbn*) cDNA was obtained by PCR from chick whole cDNA library. The following expression vectors were used in this study: pcDNA3.1-FH-N, pcDNA6/V5-His (Invitrogen), pFastBac1 (Invitrogen), pLenti6 (Invitrogen), pCS2 (+),

and pGEX6P-1 (GE Healthcare). pcDNA3.1-FH-N is a derivative of pcDNA3.1+ (Invitrogen) containing a short fragment encoding FLAG-HA sequence.

**Antibodies.** Anti-CRBN antibody was generated in rabbit against amino acids 65-76 of human CRBN. The antibody cross-reacts with mouse, rat, and zebrafish CRBN. Antibodies against FLAG (M2, Sigma), HA (3F10, Roche), V5 (V5-10, Sigma), GST (Sigma), DDB1 (Abcam), and Roc1 (Zymed) were obtained from commercial sources. Anti-Cul4A and anti-DDB2 antibodies were provided by P. Raychaudhuri (Univ. of Illinois, Chicago, IL) and T. Matsunaga, respectively.

In vitro binding assay using thalidomide-immobilized beads. Recombinant CRBN-FLAG and DDB1-V5-His proteins were expressed in Sf9 cells by using the Bac-to-bac baculovirus expression system (Invitrogen) and purified using anti-FLAG M2 agarose beads (Sigma) and Ni-NTA agarose (Qiagen), respectively. Purified CRBN-FLAG and/or DDB1-V5-His were incubated with thalidomide-immobilized beads, and bound material was eluted using SDS sample buffer. For deletion analysis of CRBN, GST-fused CRBN and its deletion mutants were expressed in E. coli BL21 cells and purified using glutathione Sepharose (GE healthcare). CRBN point mutants were overexpressed in 293T cells by transfecting appropriate FH-CRBN constructs using Lipofectamine 2000 (Invitrogen). Subsequent binding assays were carried out as described above.

**BIAcore analysis.** An amino derivative of thalidomide was conjugated to a CM5 sensor chip by using the standard amine coupling method. Various concentrations of purified CRBN-FLAG were flowed over the chip surface using a BIAcore 3000 (GE Healthcare). The resulting curves were evaluated using the BIA evaluation software, and the equilibrium dissociation constant was determined.

Coimmunoprecipitation. To investigate interactions between CRBN and DDB1, CRBN-FLAG and DDB1-V5-His were coexpressed in Sf9 cells. Cell lysates were incubated anti-FLAG agarose beads, and bound material was eluted with FLAG peptide. To purify the CRBN complex, 293T cells stably expressing FH-CRBN or its mutants were established using the lentiviral expression system (Invitrogen), and immunoprecipitation was performed as described above.

**Immunostaining.** HeLa cells overexpressing the indicated constructs were fixed, incubated with anti-HA and anti-V5 antibodies, and reacted with secondary antibodies

conjugated to Alexa Fluor 594 and 488 (Invitrogen), respectively.

In vitro ubiquitination assay. In vitro ubiquitination assays were performed essentially as described (S3). The FH-CRBN complex (0.2  $\mu$ g) was incubated at 30°C for 2 h in 15  $\mu$ l of buffer containing 0.5  $\mu$ g of Uba1 (Biomol), 0.5  $\mu$ g of UbcH5b (Biomol), 4  $\mu$ g of GST-ubiquitin (Calbiochem), and 4 mM ATP. Reactions were terminated by adding SDS and heating at 98°C for 5 min.

*In vivo* **ubiquitination assay.** The assays were performed essentially as described (*S4*). 293T cells stably expressing FH-CRBN or its mutant were treated with 10 μM MG132 for 3 h prior to harvest or left untreated. Lysates were prepared using RIPA buffer containing 25 μM MG132 and 10 mM *N*-ethylmaleimide. FH-CRBN was immunoprecipitated and analyzed as described above. Where indicated, various concentrations of thalidomide were added to cells 1 h prior to MG132 treatment.

RNAi. The following Stealth RNAi oligonucleotides (Invitrogen) were used: CRBN #1,

- 5'-CAGCUUAUGUGAAUCCUCAUGGAUA-3'; CRBN #2,
- 5'-CCCAGACACUGAAGAUGAAAUAAGU-3'; DDB1 #1,
- 5'-CAUACCUUGAUAAUGGUGUUGUGUU-3'; DDB1 #2,
- 5'-CAGUAAUGAACAAGGCUCCUAUGUA-3'; Cul4A #1,
- 5'-GCAAAGCAUGUGGAUUCAAAGUUAA-3'; Cul4A #2,
- 5'-GAAUCUCUGAUAGACAGAGACUAUA-3'. Only sense strands are shown. Stealth RNAi negative control of low GC content (Invitrogen) was also used. 293T cells were transfected with each Stealth oligonucleotide (40 nM) using Lipofectamine RNAiMAX (Invitrogen) and harvested 72 h later.

**Thalidomide treatment of zebrafish.** Fish were kept at 28.5°C on a 14-h light/10-h dark cycle, and embryos were obtained by natural matings of adult fish as described previously (*S5*). Where indicated, *fli1a:EGFP* transgenic zebrafish, which were provided by K. Kawakami (National Institute of Genetics, Mishima, Japan), were used. Zebrafish CRBN and Cul4A genes (*zcrbn* and *zcul4a*) were termed according to Zebrafish Nomenclature Guidelines by Zebrafish Nomenclature Committee. For thalidomide treatment, 400 mM stock solution was added to a final concentration of 200 or 400 μM to E3 medium prewarmed at 65°C and mixed for 1 or 2 min. Zebrafish embryos were dechorionated prior to thalidomide treatment as follows: At 2 hpf, embryos were incubated in E3 medium containing 2 mg/ml Protease type XIV (Sigma) for 3 min at room temperature and then washed five times with E3 medium. After

dechorionation, embryos were immediately transferred to E3 medium containing thalidomide and further incubated for 24 to 73 h at 28.5°C. The E3 medium was replaced with medium containing freshly prepared thalidomide every 12 h.

Alcian blue staining. Extracellular matrices associated with chondrocytes were stained using Alcian blue (*S6*). Embryos were fixed in 3.7% neutral buffered formaldehyde at room temperature for overnight and then transferred to 0.1% Alcian blue solution in 80% ethanol/20% glacial acetic acid. On the next day, stained embryos were rinsed in absolute ethanol, rehydrated to phosphate-buffered saline (PBS), and cleared with 0.05% trypsin in saturated sodium tetraborate solution for 1 to 3 h. Pigmentation was removed with 3% hydrogen peroxide/1% potassium hydroxide. Stained embryos were mounted in 70% glycerol/PBS.

## Microinjection of antisense morpholino oligonucleotides and capped mRNAs.

5'-CTGGTGCTGAACATCTTCTGCCATC-3'. These oligos were dissolved in nuclease-free water at 700  $\mu M.$ 

Whole-mount *in situ* hybridization. Whole-mount *in situ* hybridization was carried out essentially as described (*S7*). Antisense probe for *zcrbn* mRNA was directed against the 5' coding region of 513 bases. Antisense probe for *zcul4a* mRNA was directed against the 3' UTR of 590 bases. Probes for *sonic hedgehog (shh)* and *fgf8a* mRNAs were provided by S. Krauss (Institute of Medical Microbiology, Oslo, Norway) and B. Thisse (Univ. of Virginia, Charlottesville, VA), respectively. To increase permeability of probes, fixed embryos were incubated with PBS containing 0.1% Tween 20 and 10 μg/ml proteinase K for 2 min at room temperature.

**Measurement of otic vesicle size.** 30-hpf embryos were anesthetized in 1% methylcellulose containing 0.003% 3-amino benzoic acid ethyl ester (Sigma). When a large number of samples were processed, embryos were fixed in 3.7% formaldehyde and, prior to inspection, re-equilibrated in PBS containing 0.5% Triton X-100. Images

of the embryos (lateral view) were then collected using a digital camera. The length of the long axis of the otic vesicle and the body length of the embryo were measured using Adobe Photoshop, and otic vesicle size was reported as a ratio to the size of the embryo. From the averages and the standard deviations of the data, p-values were determined using the Mann-Whitney U test.

Analyses of chick embryos. Chick fertilized eggs were obtained from the Yamagishi poultry farm. Staging of embryos was performed as described previously (*S8*). Electroporation into the lateral plate mesoderm was carried out as described previously (*S9*). Briefly, 3 mg/ml pcDNA3.1-FH-CRBN and 0.8 mg/ml pCAGGS-EGFP were coinjected into the forelimb field at stage 14 by using a fine glass-pipette needle, and electric pulses were applied (8 V, 60 ms on and 50 ms off, repeated three times). At 12 h post-transfection, 50 µl of 3.9 mM thalidomide in DMSO:PBS (1:7) or vehicle alone was directly applied onto one of the forelimb buds at stage 19 (*S10*). At stage 36, skeletal cartilages were visualized by Victoria blue staining, followed by clearing with methyl salycilate (*S11*). Non-radioactive whole-mount *in situ* hybridization analysis of chick embryos was carried out as described (*S12*). Antisense probes for *Fgf10* and *Fgf8* mRNAs were provided by S. Noji (Univ. of Tokushima, Tokushima, Japan) and J. C. Izpisua-Belmonte (Salk Institute, San Diego, CA), respectively.

#### SUPPORTING TEXT

Influence of the timing of thalidomide administration to zebrafish. It has been shown that the thalidomide-sensitive period (20 to 36 days post conception in humans and around Hamburger-Hamilton stages 17 to 19 in chick) coincides with the commencement of limb bud outgrowth in these species and with the timing at which Fgf8 expression starts to increase in the chick AER (S10, S13). In zebrafish, pectoral fin buds are formed at around 30 hpf, whereas fgf8 expression in the AER is only detectable at 36 hpf (S14). To narrow down the thalidomide-sensitive period in zebrafish, we carried out time-course experiments (fig. S10E). Incidence and severity of fin malformations were similarly high when thalidomide was added at 1 or 12 hpf. When thalidomide was added at 24 hpf, the incidence and severity were significantly lower, although still noticeable. Hence, there seems to be a gap between the thalidomide-sensitive period and fin development in zebrafish. The apparent inconsistency may be related to the problem with drug penetration. This problem has

been described in the study of many other compounds (*S15*). Thus, thalidomide may penetrate inefficiently or slowly into zebrafish embryos, especially at later stages, by waterborne exposure. In support, while at the 3-somite stage (11 hpf), there is no epidermis covering the embryo that might act as a diffusion barrier, the epidermis is thick for ages over one day. In any case, it does not seem that "bathing" experiments provide relevant information on dose response and time course.

A more detailed look at the phenotypes induced by thalidomide in zebrafish. Fish have an ear as the hearing and balance organ, which is similar in many ways to the inner ear of amniotes, but they do not have an outer or middle ear structure. Hence, ear malformation in zebrafish can only be manifested as a reduction of the otic vesicle in size, whereas in humans thalidomide also induces malformations to the outer and middle ear.

Tetrapod limbs and fish pectoral fins are homologous with respect to early patterning of limb/fin buds and gene expression therein, although skeletal structures in the adult are quite different. From the studies in chicks and mammals, the AER at the distal tip of the limb bud appears to play an important role in outgrowth of the limb and in endoskeletal patterning along the proximodistal axis. The AER facilitates elongation of the limb bud by promoting proliferation of mesenchymal cells and by regulating expression of other signaling molecules. Secreted factors such as Fgf4 and Fgf8 are expressed in the AER and mediate its functions.

In zebrafish, packages of dense mesenchymal cells called chondrogenic condensations are formed within pectoral fin buds by 37 hpf (S16). Chondrogenic condensations then give rise to the pectoral girdle and the endoskeletal disc. During the larval period, the endoskeletal disc is divided into four cartilaginous elements, called proximal radials, through decomposition of cartilage matrix. During the following two weeks, the larval pectoral fins continue to grow while their larval structure is maintained, and in the third week of development, extensive reconstructions and expansions, including formation of distal radials, occur.

What we found in thalidomide-treated 48- to 75-hpf zebrafish embryos are (i) shortening of pectoral fins along the proximodistal axis, (ii) reduction of fgf8a expression in the AER, and (iii) reduction of endoskeletal disc in size. These results may be interpreted to suggest that reduction of fgf8a expression prevented proliferation and differentiation of chondrogenic condensations. Consistent with this, thalidomide is reported to induce mesenchymal cell death in the chick limb bud (S17). Because skeletal structures are quite different between limbs and fins, it cannot be stated whether the thalidomide-induced morphological changes in zebrafish are similar to phocomelia or

amelia.

Anti-angiogenic effect of thalidomide on zebrafish pectoral fin buds. To determine whether and when thalidomide affects vasculogenesis in thalidomide-sensitive tissues in zebrafish, we monitored vasculogenesis in pectoral fin buds using fli1a:EGFP transgenic fish, in which EGFP is expressed in vascular endothelial cells (fig. S18). It is reported that the marginal blood vessel (MBV) is formed at the distal part of developing pectoral fin buds between 46 and 57 hpf (S16), and it is only at 52 or 54 hpf that blood circulation starts there (S18). In agreement with the earlier studies, the presence of the MBV looping around the bud was evident at 52 hpf (fig. S18H), but not at 47 hpf (fig. S18B), and thalidomide inhibited MBV formation at 52 hpf (fig. S18K). Remarkably, however, thalidomide-treated embryos exhibited developmental defects in the fin buds already at 47 hpf, when the MBV was still absent (fig. S18, A and D). Moreover, in 48-hpf embryos, fgf8 expression was reduced by thalidomide treatment or knockdown of zCrbn or zCul4a (Fig. 5 and fig. S14). Hence, our data suggest that these morphological and transcriptional changes in pectoral fin buds precede inhibition of vasculogenesis and are therefore not secondary to the anti-angiogenic effect of thalidomide. By contrast, a recent study suggested anti-angiogenic activity of thalidomide as a primary cause of chick limb malformations, demonstrating that thalidomide-induced inhibition of vasculogenesis precedes inhibition of Fgf8 expression and cell death in limb buds (S10). Therefore, the sequence of events induced by thalidomide may be different in these species. These observations are concordant with the common view of species differences in thalidomide action (see below). Chick and zebrafish may have completely different mechanisms of thalidomide action, with different primary target tissues. Alternatively, thalidomide may directly induce multiple independent events (e.g., vascular defects and fgf8 downregulation), the order of which is different due to species-specific differences in developmental programs.

**Species differences in thalidomide sensitivity.** Thalidomide shows teratogenic activity in humans, rabbits, chicks, and zebrafish, but not in mice and rats. Below we discuss various possibilities for the species differences in light of our new findings. CRBN is evolutionarily conserved (fig. S8), and thalidomide binds to CRBN from humans, mice, chick, and zebrafish (figs. S2, S13, and S17). Hence, CRBN is unlikely to be related to the species specificity.

First, pharmacokinetic differences may be an underlying cause of the species differences. Thalidomide is rapidly hydrolyzed or metabolized to over a dozen products *in vitro* and *in vivo* (S19-S21), and many of the breakdown products are nonteratogenic

(S10). In support of the above idea, plasma elimination half-life of orally administered thalidomide is significantly shorter in mice ( $\sim$ 0.5 h) than in rabbits ( $\sim$ 2.2 h) and humans ( $\sim$ 7.3 h) (S21). However, one may argue that this explanation is unlikely because thalidomide does not cause limb defects in mice at any dose tested (S22).

Conversely, metabolic breakdown in the liver may be required for thalidomide to be active, and this bioactivation may occur in a species-specific manner. This model is based on the observation that thalidomide shows its anti-angiogenic effect in aortic ring assay in the presence of human or rabbit liver microsomes, but not in the presence of rat liver microsomes (*S23*, *S24*). As discussed above, however, thalidomide seems to induce morphological and transcriptional changes independently of its anti-angiogenic effect in zebrafish. Moreover, as discussed below, there is evidence suggesting that the liver is not involved in teratogenic action of thalidomide in zebrafish and chick. Furthermore, the bioactivation model is inconsistent with the observation that the parent thalidomide molecule binds to CRBN and inhibits its function *in vitro*.

Third, thalidomide-induced formation of reactive oxygen species is reported to occur in rabbits but not in mice (*S25*, *S26*). Fourth, interspecies differences in gestational development may result in different developmental toxic manifestations after exposure to thalidomide (*S22*).

Effective concentrations of thalidomide *in vitro* and *in vivo*. Typical doses used for leprosy and multiple myeloma are 50 to 800 mg per day, and at these doses, thalidomide also exerts its sedative and teratogenic effects. Based on a single-compartment model, in which a drug is evenly distributed throughout the plasma and tissues, thalidomide concentrations in the body are assumed to be 3 to 48  $\mu$ M, and the lower range of these figures is in fact close to 5.4  $\mu$ M, the mean peak plasma concentration in patients to which 2 to 4 mg/kg of thalidomide was given (*S21*). Thalidomide was added to our ubiquitination assays at 10 to 100  $\mu$ M and showed a significant inhibitory effect at 10  $\mu$ M (Fig. 3). These results are therefore consistent with the idea that the inhibitory effect of thalidomide is associated with its other activities *in vivo*.

On the other hand, thalidomide was used at 200 or 400  $\mu$ M in our zebrafish experiments. These concentrations were determined empirically based on the phenotypes induced. Thalidomide caused a similar inhibitory effect on fin development at 200 and 400  $\mu$ M (fig. S10E). Similarly, in Yabu *et al.* (*S27*), thalidomide was used at 100 to 800  $\mu$ M, and its anti-angiogenic effect was observed at or more than 200  $\mu$ M. We observed no symptom of acute toxicity in our animal experiments. According to Radomsky and Levine (*S28*), thalidomide does not have any acute toxicity, and fatal overdose is virtually impossible. In comparison, in rabbits, teratogenic and

anti-angiogenic effects have been observed by oral administration of thalidomide at 100 to 400 mg/kg, or 385 to 1,540 µM in a single-compartment model (*S22*, *S25*, *S29*, *S30*). Thus, effective concentrations of thalidomide seem to vary substantially even among thalidomide-sensitive species, and thalidomide sensitivity of zebrafish seems to be one order of magnitude lower than that of humans.

In our chick experiments, thalidomide was used at 50  $\mu$ g per egg or 780  $\mu$ g/kg. This amount is similar to those used in previous papers (S10, S17) and is equal to 3.1  $\mu$ M in a single-compartment model. In fact, however, its concentration in target tissues is likely to be much higher because 3.9 mM stock solution was directly applied to one of the forelimb buds. A similar application method was also employed by others (S10). Diffusion of the drug should occur to some extent but not fully, because thalidomide caused specific developmental defects in the thalidomide-treated limb, but not in the other limbs. For this reason, effective concentrations of thalidomide in chick cannot be deduced precisely.

Possible breakdown of thalidomide in our assays. Since thalidomide was heated at 65°C to dissolve the solid compound and then left in culture medium for up to 12 h at 28.5°C, we concerned about enzymatic and/or nonenzymatic breakdown of thalidomide. Therefore, the levels of thalidomide was monitored by HPLC as described previously (S31). At the time of addition to zebrafish embryos, 98% of thalidomide was found to remain intact. After 12 h of incubation in zebrafish E3 medium, 85% of thalidomide remained intact. Hydrolysis is unlikely to occur in DMSO. It is also reported that hydrolysis is dependent on pH and is slow to occur under mildly acidic conditions (S31). As the pH of E3 medium is 6.5 to 6.9, our finding does not conflict with earlier studies. It should also be noted that developmental defects of otic vesicles were observed at 30 hpf, when the liver is at an early stage of its development and is not yet functional. hnf4, one of the key transcription factors responsible for hepatic transcription of the P450 genes, remains to be expressed at 30 hpf, and vascularization that is essential for liver function occurs only after 60 hpf (S32). It is therefore reasonable to assume that the parent thalidomide molecule was a major cause of the developmental defects we observed, although it is possible that minor hydrolyzed products and/or metabolites generated in tissues other than the liver were involved.

In chick, as stated above, a concentrated stock solution was directly applied to one of the forelimb buds, and this caused specific developmental defects in the thalidomide-treated limb, but not in the other limbs. Moreover, the liver is premature and not yet fully functional at the stages examined. It is therefore unlikely that metabolism in the liver was involved under our experimental conditions. Evidently,

however, it is possible that enzymatic or nonenzymatic breakdown of thalidomide occurred locally and that breakdown products contributed to the developmental defects.

For the above reasons, we assume that the teratological outcomes observed in zebrafish and chick can be due to the parent thalidomide molecule. It is, however, practically impossible to demonstrate this point unequivocally *in vivo*. From a CRBN-centric perspective, the observations that the parent molecule binds to CRBN and inhibits its function and that the teratogenic effects are suppressed by overexpression of a thalidomide-binding-deficient mutant of CRBN suggest that thalidomide or its breakdown products retaining CRBN-binding activity are involved in the teratogenic effects. Many of the breakdown products are thought to be nonteratogenic (*S10*). Further study on the relationship between teratogenicity and CRBN-binding activity of thalidomide breakdown products may shed new light on the above issue.

# $\label{lem:connection} \textbf{Possible connection between CRBN and thal idomide-induced oxidative stress.} \ It$

has been shown that thalidomide facilitates the formation of reactive oxygen species and thereby causes oxidative DNA damage (*S25*). However, the idea that the damaged DNA-binding protein DDB1 may link CRBN to the oxidative stress is not supported by our data. DDB1 and DDB2 form the DDB complex. While DDB2 directly binds damaged DNA, the role of DDB1 in DNA damage response is still unclear. Despite its name, DDB1 is better characterized as a component of E3 ubiquitin ligase complexes, and DDB1 is thought to be recruited to damaged DNA sites through binding to DDB2. Here we showed that CRBN binds to DDB1 but not to DDB2, and that CRBN and DDB2 in fact bind to DDB1 in a competitive manner (Fig. 2C). Hence, CRBN probably functions independently of the DDB2-mediated DNA damage response pathway.

### Possible connection between CRBN and tissue specificity of thalidomide action.

Below we discuss how our findings might explain tissue specificity of thalidomide action. In 48-hpf embryos, *zcrbn* is highly expressed at pectoral fin, brain, and head vasculature, whereas its expression is not detectable in somites (fig. S12). *zcrbn* expression at pectoral fin and head regions is consistent with it being a mediator of thalidomide teratogenicity. By contrast, CRBN appears to be ubiquitously expressed in adult human and mouse tissues (*S33*). CRBN is necessary, but evidently not sufficient, for thalidomide teratogenicity, and other molecules, such as downstream targets of CRBN, are also likely to be required. Then, tissue specificity in thalidomide teratogenicity may be defined in part by expression patterns of such molecules, and in this respect, Fgf8 is particularly interesting.

Originally, a nonsense mutation of CRBN that causes a small C-terminal deletion (R419X) was found associated with mild mental retardation in a large kindred (S34). Later, rat CRBN was found to bind to the large-conductance calcium-activated potassium channel, a.k.a. Slo, and regulate its activity (S35, S36). Coincidently, mice lacking Slo show cerebellar dysfunction, possibly due to reduced activity of cerebellar Purkinje neurons, although the mutant mice do not manifest any gross morphological abnormalities (S37). Hence, Slo may play an important role in the function of CRBN in the brain (perhaps only in the brain). As to the effects of thalidomide on the brain, thalidomide is associated with mental retardation, although its incidence is low (S13). Currently we are investigating a possible interplay between thalidomide and CRBN in the brain.

CRBN as a new substrate receptor of an E3 ubiquitin ligase complex. Our findings support the idea that CRBN functions as a substrate receptor subunit of a DDB1-Cul4A-Roc1-containing E3 ubiquitin ligase complex. First, CRBN and DDB2, the known substrate receptor, bind competitively to DDB1. Second, CRBN undergoes auto-ubiquitination as do many other substrate receptors. Whereas many substrate receptors of DDB1-Cul4 complexes, including DDB2, possess a conserved WDXR motif (\$38\$), a few substrate receptors are known to lack this motif (\$4, \$39, \$40\$). As CRBN does not have an identifiable WDXR motif, this protein might be a substrate receptor of the latter type. As additional evidence for the above idea, we also showed that knockdown of CRBN or Cul4A caused similar developmental defects in zebrafish. However, the Cul4A knockdown resulted in a more severe phenotype in fin development. This observation is not surprising, since CRBN is only one of several substrate receptors associated with the DDB1-Cul4-Roc1 complex.

Clinical implications. Thalidomide was originally prescribed as a sedative, but is now used for the treatment of multiple myeloma and leprosy. In addition, one of its derivatives called lenalidomide is in a clinical trial for a different type of cancer called myelodisplastic syndrome (*S41*). Whether CRBN is involved not only in teratogenicity but also in these pharmacological effects of thalidomide is unclear. At present, it is tempting to speculate pharmacological inhibition of CRBN activity might be involved in the therapeutic action of thalidomide in multiple myeloma because Bortezomib, a selective proteasome inhibitor, is an effective agent for multiple myeloma (*S42*, *S43*). In this scenario, drug screening in CRBN-binding and ubiquitination assays may lead to the discovery of more effective thalidomide derivatives. If, on the contrary, CRBN is not involved in the beneficial effects of thalidomide, its nonteratogenic derivatives

could be designed rationally. In any event, development of such derivatives could be of considerable clinical significance because thalidomide provides effective therapy for several diseases that are difficult to treat by other means.

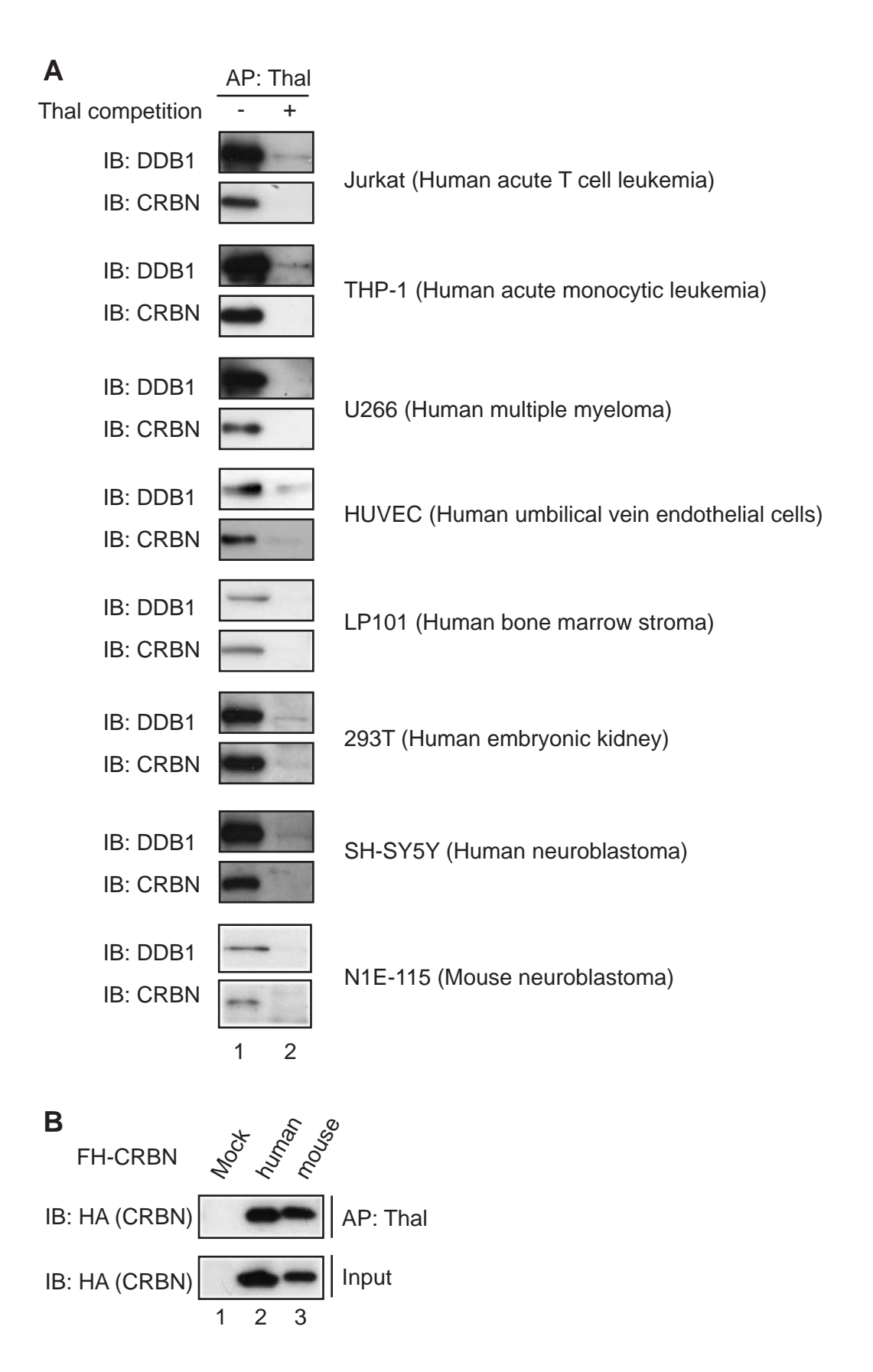
### SUPPORTING REFERENCES

- S1. S. Sakamoto, Y. Kabe, M. Hatakeyama, Y. Yamaguchi, H. Handa, *Chem. Rec.* **9**, 66 (2009).
- S2. H. Uga et al., Mol. Pharmacol. 70, 1832 (2006).
- S3. R. Groisman et al., Cell 113, 357 (2003).
- S4. F. Ohtake et al., Nature 446, 562 (2007).
- S5. H. Ando, T. Furuta, H. Okamoto, Methods Cell Biol. 77, 159 (2004).
- S6. W. L. Kelly, M. M. Bryden, Stain Technol. 58, 131 (1983).
- S7. C. Thisse, B. Thisse, *Nat. Protoc.* **3**, 59 (2008).
- S8. V. Hamburger, H. Hamilton, *J. Morphol.* **88**, 49 (1951).
- S9. T. Suzuki, T. Ogura, *Dev. Growth Differ.* **50**, 459 (2008).
- S10. C. Therapontos, L. Erskine, E. R. Gardner, W. D. Figg, N. Vargesson, *Proc. Natl. Acad. Sci. U.S.A.* **106**, 8573 (2009).
- S11. T. Suzuki, S. M. Hasso, J. F. Fallon, *Proc. Natl. Acad. Sci. U.S.A.* **105**, 4185 (2008).
- S12. M. A. Nieto, K. Patel, D. G. Wilkinson, Methods Cell Biol. 51, 219 (1996).
- S13. M. T. Miller, K. Stromland, *Teratology* **60**, 306 (1999).
- S14. F. Reifers et al. Development 125, 2381 (1998).
- S15. R. D. Murphey, H. M. Stern, C. T. Straub, L. I. Zon, *Chem. Biol. Drug Des.* **68**, 213 (2006).
- S16. H. Grandel, S. Schulte-Merker, *Mech. Dev.* **79**, 99 (1998).
- S17. J. Knobloch, J. D. Shaughnessy, Jr., U. Ruther, FASEB J. 21, 1410 (2007).
- S18. C. B. Kimmel, W. W. Ballard, S. R. Kimmel, B. Ullmann, T. F. Schilling, *Dev. Dyn.* **203**, 253 (1995).
- S19. M. Melchert, A. List, Int. J. Biochem. Cell Biol. 39, 1489 (2007).
- S20. M. E. Franks, G. R. Macpherson, W. D. Figg, Lancet 363, 1802 (2004).
- S21. F. Chung et al., Clin. Cancer Res. 10, 5949 (2004).
- S22. G. Janer, W. Slob, B. C. Hakkert, T. Vermeire, A. H. Piersma, *Regul. Toxicol. Pharmacol.* **50**, 206 (2008).
- S23. Y. Ando, E. Fuse, W. D. Figg, Clin. Cancer Res. 8, 1964 (2002).

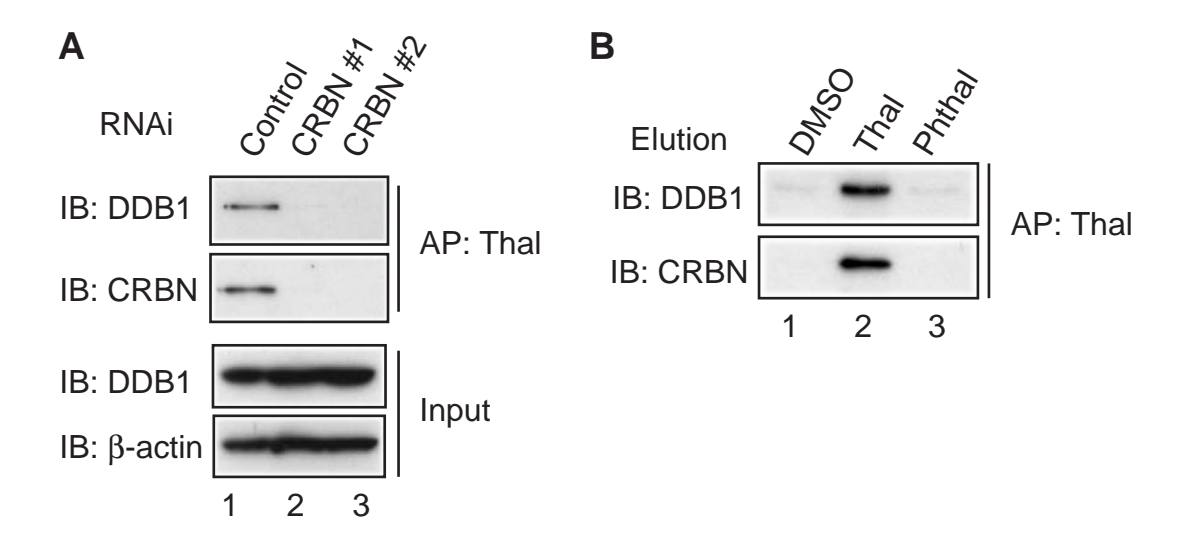
- S24. K. S. Bauer, S. C. Dixon, W. D. Figg, *Biochem. Pharmacol.* 55, 1827 (1998).
- S25. T. Parman, M. J. Wiley, P. G. Wells, *Nat. Med.* **5**, 582 (1999).
- S26. J. Knobloch, K. Reimann, L. O. Klotz, U. Ruther, *Mol. Pharm.* 5, 1138 (2008).
- S27. T. Yabu et al., Blood 106, 125 (2005).
- S28. C. Radomsky, N. Levine, *Derm. Clin.* **19**, 87 (2001).
- S29. R. J. D'Amato, M. S. Loughnan, E. Flynn, J. Folkman, *Proc. Natl. Acad. Sci. U.S.A.* **91**, 4082 (1994).
- S30. H. Sterz, H. Nothdurft, P. Lexa, H. Ockenfels, Arch. Toxicol. 60, 376 (1987).
- S31. S. Zhou, Y. Li, P. Kestell, J. W. Paxton, J. Chromatogr. B Analyt. Technol. Biomed. Life Sci. 785, 165 (2003).
- S32. H. A. Field, P. D. Dong, D. Beis, D. Y. Stainier, Dev. Biol. 261, 197 (2003).
- S33. A. I. Su et al., Proc. Natl. Acad. Sci. U.S.A. 101, 6062 (2004).
- S34. J. J. Higgins, J. Pucilowska, R. Q. Lombardi, J. P. Rooney, *Neurology* **63**, 1927 (2004).
- S35. S. Jo, K. H. Lee, S. Song, Y. K. Jung, C. S. Park, J. Neurochem. 94, 1212 (2005).
- S36. J. J. Higgins, J. Hao, B. E. Kosofsky, A. M. Rajadhyaksha, *Neurogenetics* **9**, 219 (2008).
- S37. M. Sausbier et al., Proc. Natl. Acad. Sci. U.S.A. 101, 9474 (2004).
- S38. J. Jin, E. E. Arias, J. Chen, J. W. Harper, J. C. Walter, Mol. Cell 23, 709 (2006).
- S39. S. Angers et al., Nature 443, 590 (2006).
- S40. O. Leupin, S. Bontron, M. Strubin, J. Virol. 77, 6274 (2003).
- S41. A. List et al., N. Engl. J. Med. 352, 549 (2005).
- S42. J. Adams et al., Bioorg. Med. Chem. Lett. 8, 333 (1998).
- S43. T. Hideshima et al., Cancer Res. 61, 3071 (2001).

Fig. S1. Scheme of thalidomide immobilization to FG beads. (A and B) Structure of thalidomide and its derivative, FR259625. (C) Scheme of thalidomide immobilization to FG beads is shown. Details are described in Materials and Methods.

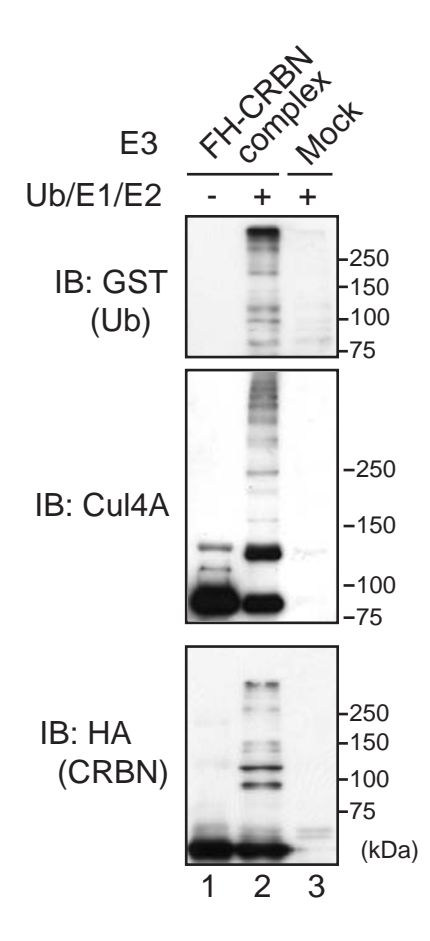
FG beads



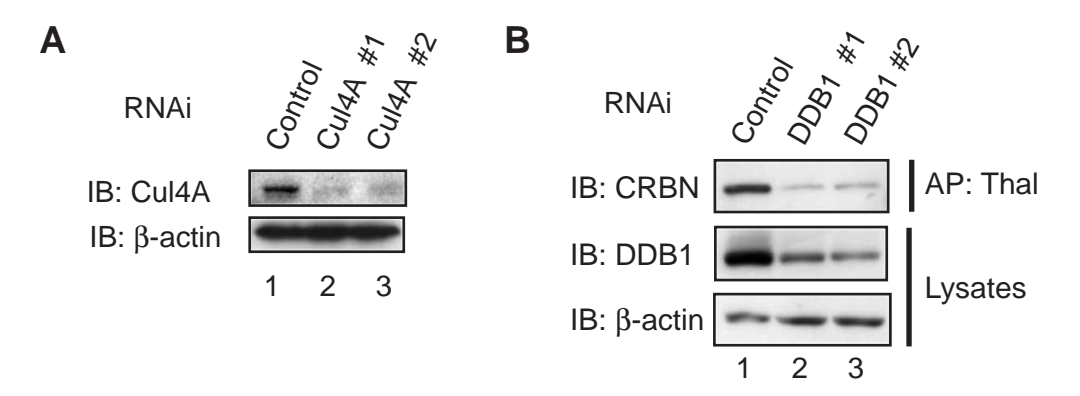
**Fig. S2.** Species- and cell type-independent interaction of CRBN and DDB1 with thalidomide. (**A**) Extracts prepared from the indicated cell lines were subjected to affinity purification (AP) with thalidomide (Thal)-immobilized beads. Where indicated, 0.3 mM thalidomide was added to extracts prior to incubation with the beads. (**B**) Extracts prepared from 293T cells overexpressing FH-CRBN of human or mouse origin were similarly subjected to affinity purification with thalidomide beads. Lysates (input) and affinity-purified materials were immunoblotted (IB) using the indicated antibodies.



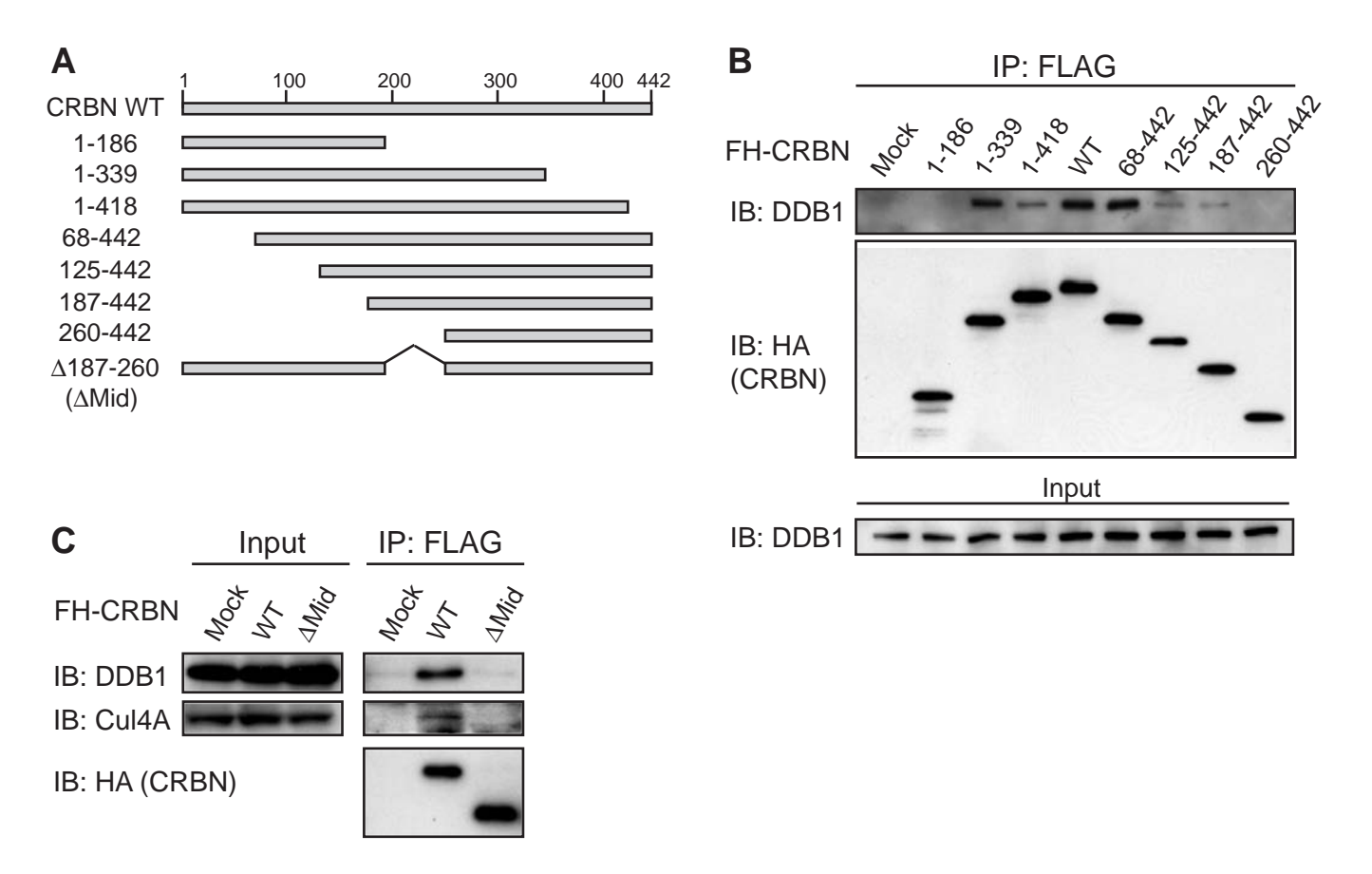
**Fig. S3.** DDB1 binds to thalidomide indirectly through CRBN, but DDB1 and CRBN do not bind to phthalimide appreciably. (**A**) 293T cells were transfected with CRBN or control siRNA, and the resulting cell lysates were subjected to affinity purification (AP) with thalidomide (Thal) beads. Lysates (input) and affinity-purified materials were immunoblotted (IB). Knockdown efficiency of the siRNAs used is summarized in table S2. (**B**) Following affinity purification with thalidomide beads, bound proteins were eluted with free thalidomide or phthalimide (Phthal).



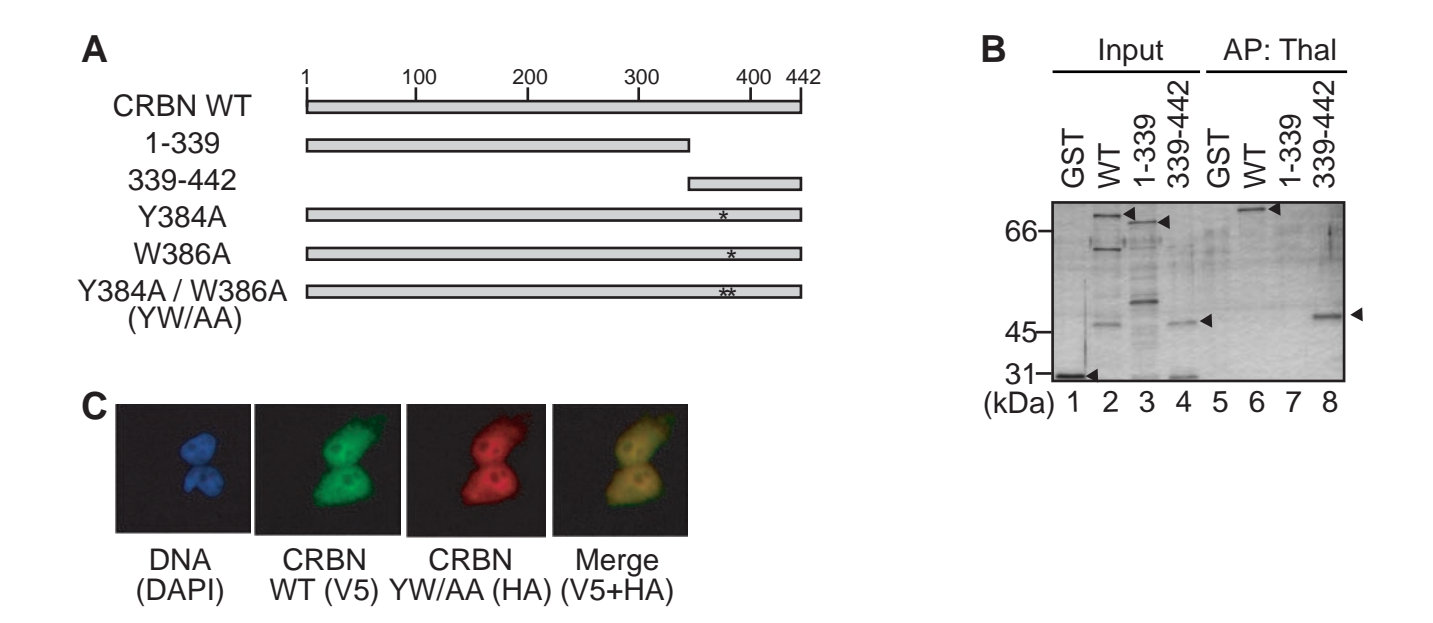
**Fig. S4.** Ubiquitination of the CRBN complex *in vitro*. The FH-CRBN complex purified from 293T cells stably expressing FH-CRBN was incubated with or without GST-ubiquitin (Ub), Uba1 (E1), UbcH5b (E2), and ATP, and aliquots of the reactions were immunoblotted (IB) with the indicated antibodies. Mock, mockpurified materials from control cells.



**Fig. S5.** Knockdown of Cul4A (**A**) and DDB1 (**B**) in 293T cells. 293T cells were transfected with Cul4A, DDB1, or control siRNA, and the resulting lysates were immunoblotted (IB). Knockdown efficiency of the siRNAs used is summarized in table S2. Affinity purification (AP) was also carried out using thalidomide (Thal) beads because CRBN in cell lysates is hardly detectable by immunoblotting and enrichment is necessary for its detection. CRBN is quantitatively recovered by this procedure. The data in (B) suggest that knockdown of DDB1 leads to a substantial reduction of the CRBN protein level.



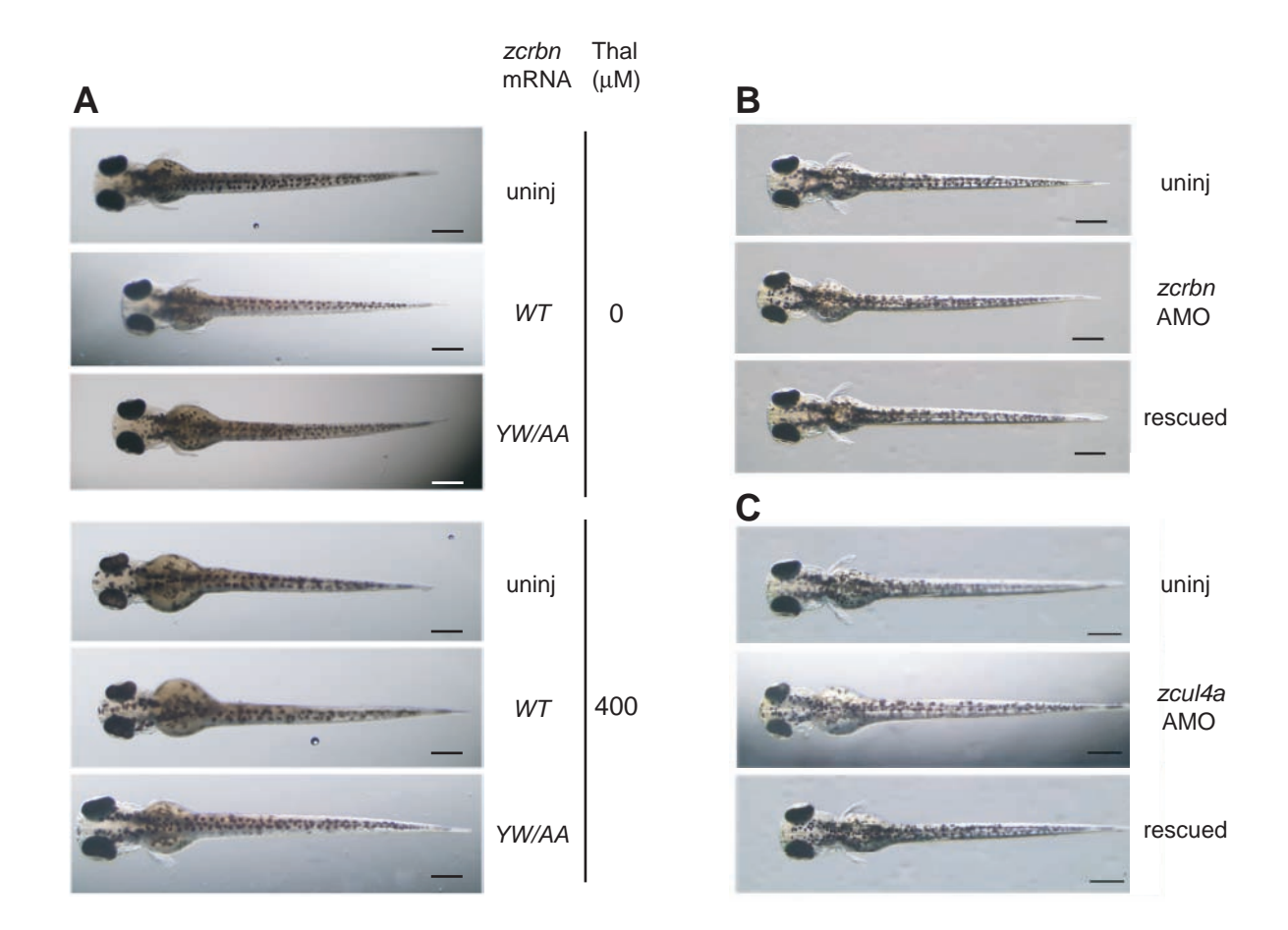
**Fig. S6.** A central 74-amino acid region of CRBN is critical to DDB1 binding. (**A**) Schematic representation of CRBN and its deletion mutants. (**B** and **C**) FH-CRBN and its mutants were expressed in 293T cells and immunoprecipitated (IP) with anti-FLAG antibody. Lysates (input) and immunoprecipitates were immunoblotted, and FH-CRBN and coprecipitated endogenous DDB1 were detected.



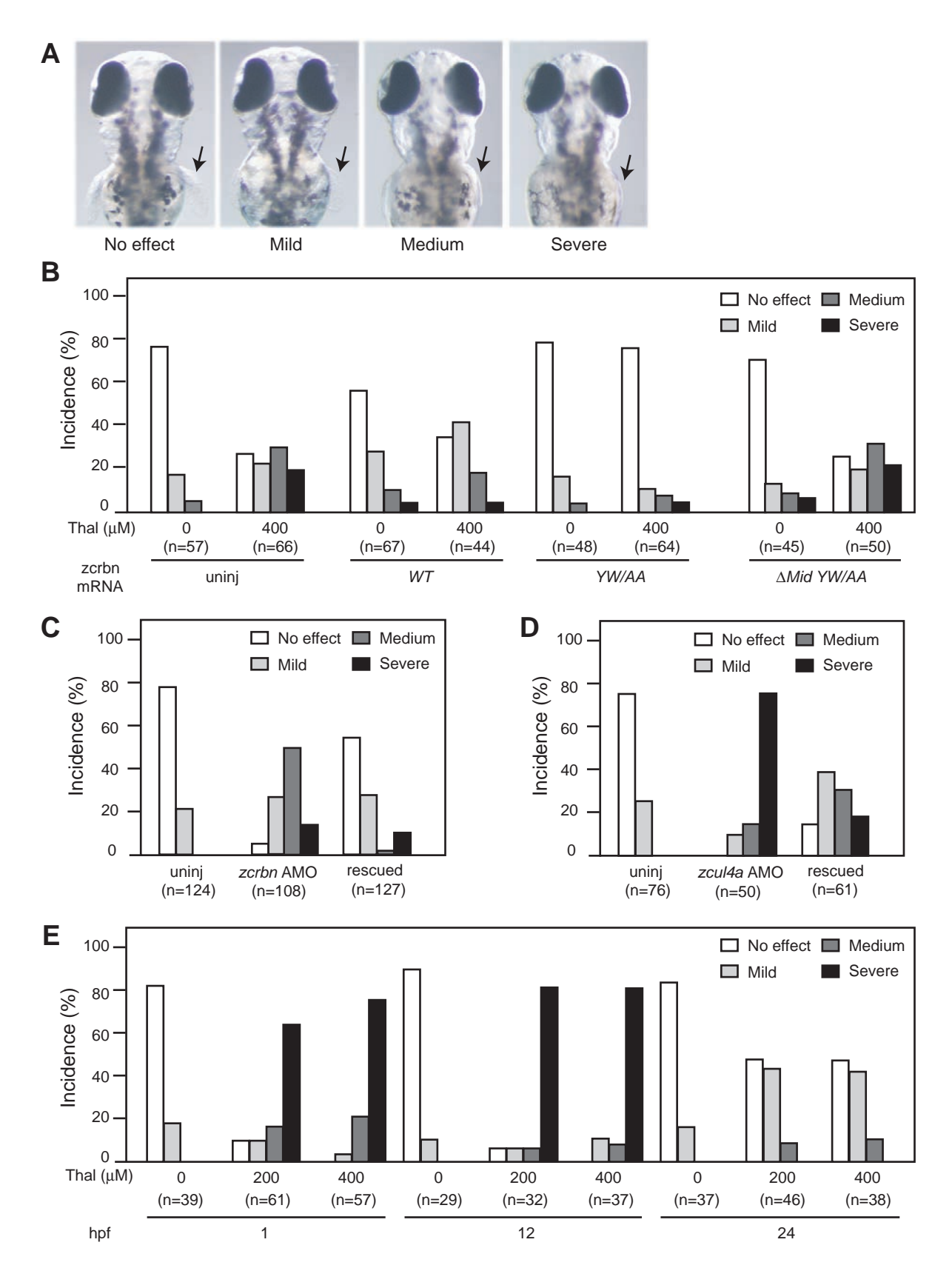
**Fig. S7.** The C-terminal region of CRBN comprising amino acids 339-442 is responsible for thalidomide binding. (**A**) Schematic structure of CRBN mutants. Asterisks indicate the positions of alanine substitutions. (**B**) GST-CRBN proteins were incubated with thalidomide-immobilized beads. Input and affinity-purified (AP) samples were stained with silver. The positions of full-length GST-fusion proteins are indicated by arrowheads. (**C**) CRBN-V5-His and FH-CRBN<sup>YW/AA</sup> were coexpressed in HeLa cells and immunostained. DAPI, 4',6-diamidino-2-phenylindole.

	<b>←</b>	
Homo sapiens	326: C QETEITT-KNEIFSLSLC G PMAA Y V NP H G Y V H E TL T V Y KACNLNLI G R P STEH SWFP	382
Mus musculus	329:CQETEITT-KNEIFSLSLCGPMAAYVNPHGYVHETLTVYKASNLNLIGRPSTVHSWFP	385
Gallus gallus	328:CQDTEITT-KNEIFSLSLCGPMAAYVNPHGYIHETLTVYKACNLNLSGRPSTEHSWFP	384
Danio rerio	316:CQDTEITS-KNEIFSLSLYGPMAAYVNPHGYVHETLTVYKASNLNLIGRPSTLHSWFP	372
D. melanogaster	458: CNSSLALCSDLFAMSKHGVQTQYCNPEGYIHETNTVYRVISHAIGYSGEPSTKFSWFP	515
A. thaliana	447: CQTVI-ARRK-DMLVMSNEGPLGAYVNPHGYVHEIMTFYKANDIALRGRPVKKDSWFP	502
	* *	
Homo sapiens	383:GYAWTVAQCKICASHIGWKFTATKKDMSPQKFWGLTRSALLPTIPDTEDEISPD	436
Mus musculus	386:GYAWTIAQCKICASHIGWKFTATKKDMSPQKFWGLTRSALLPTIPETEDEISPD	439
Gallus gallus	385:GYAWTIAQCRICGNHMGWKFTATKKDMSPQKFWGLTRSALLPRIPEAEDELGHD	438
Danio rerio	373:GYAWTIAQCRTCSSHMGWKFSAVKKDLSPPRFWGLTRSALLPTIPQGEEGVEGS	426
D. melanogaster	516:GYQWHIILCKFCAQHVGWEFKAVHPNLTPKVFFGLAGSSVRIGKASEYSPFNGTTYVVRN	575
A. thaliana	503:GYAWTIANCATCETQLGWHFTATNKKLKPSSFWAVRGSQVA-DDM	546
	<del></del>	
Homo sapiens	437:KVI-LCL-	442
Mus musculus	440:KVI-LCL-	445
Gallus gallus	439:RSPLLCL-	445
Danio rerio	427:RLLCL-	431
D. melanogaster	576:MMRMISSDME	585
A. thaliana	547:R	547

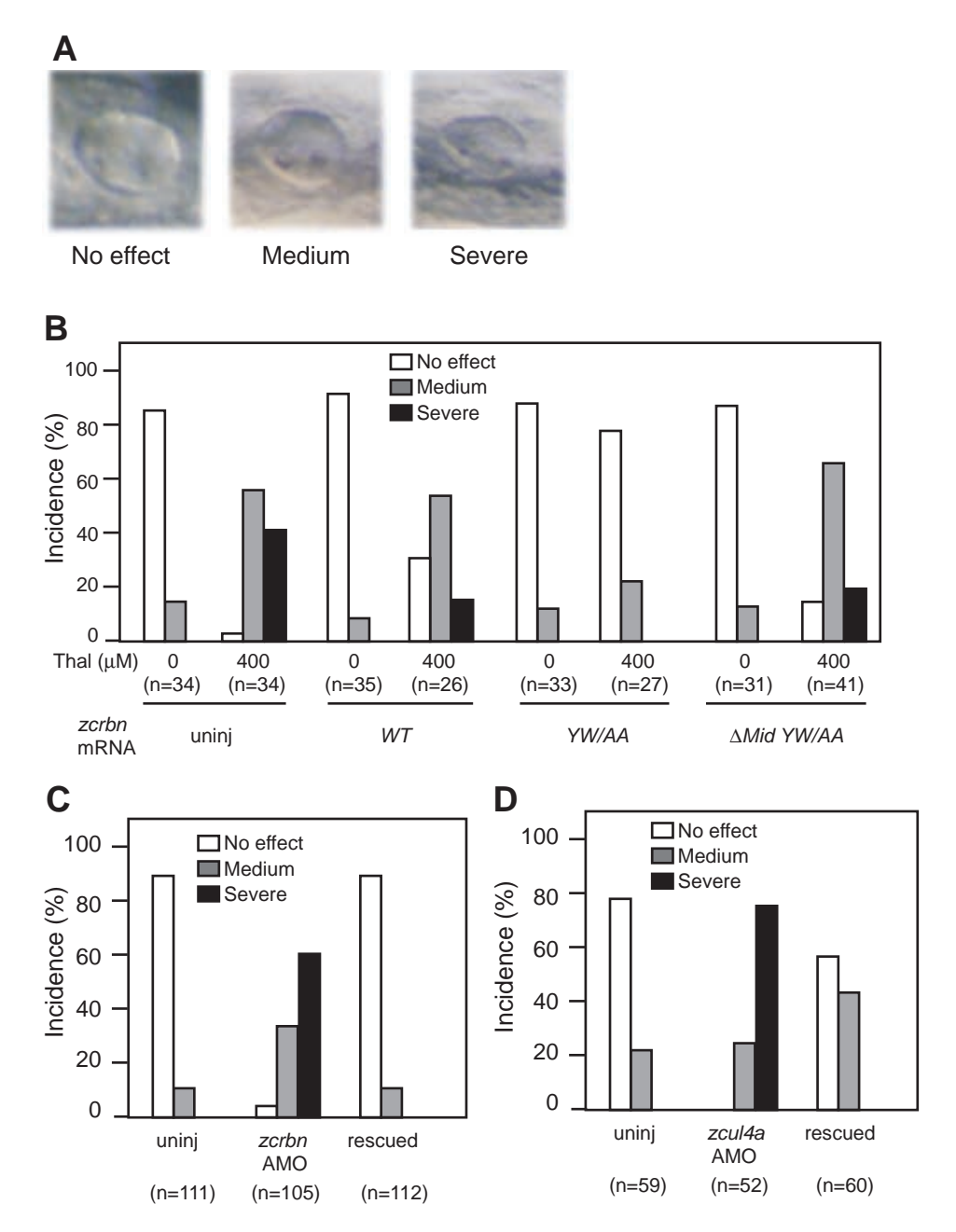
**Fig. S8.** Evolutionary conservation of CRBN. Amino acid sequences of CRBN orthologs from six species are aligned. Bold letters indicate amino acids that are fully conserved among these species. Arrow indicates the thalidomide-binding region determined by deletion analysis, whereas asterisks indicate amino acids that are critical for thalidomide binding (see Fig. 3 and fig. S7).



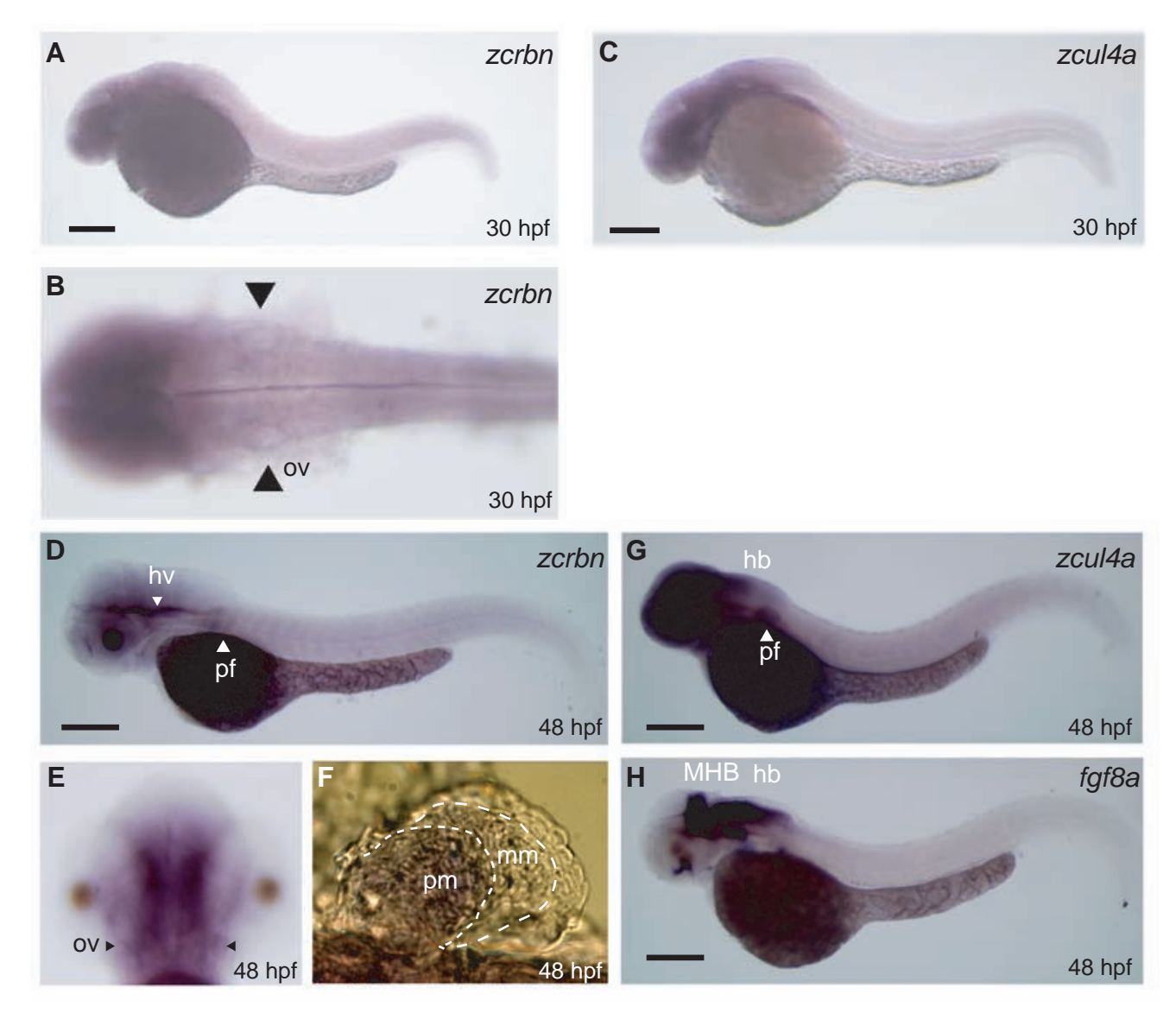
**Fig. S9.** Lack of general growth retardation in zebrafish treated with thalidomide or injected with *zcrbn* or *zcul4a* AMO. (**A**) Control embryos (uninj) or embryos injected with *zcrbn* mRNA were grown in the presence or absence of thalidomide. (**B** and **C**) Control embryos (uninj), embryos injected with the indicated AMOs, or embryos injected with the AMOs and the corresponding mRNAs (rescued) were examined. Representative dorsal views of 72-hpf embryos are shown. (A), (B), and (C) serve as controls for Fig. 5A, 4C, and 4E, respectively. uninj, uninjected. Scale bar, 250 μm.



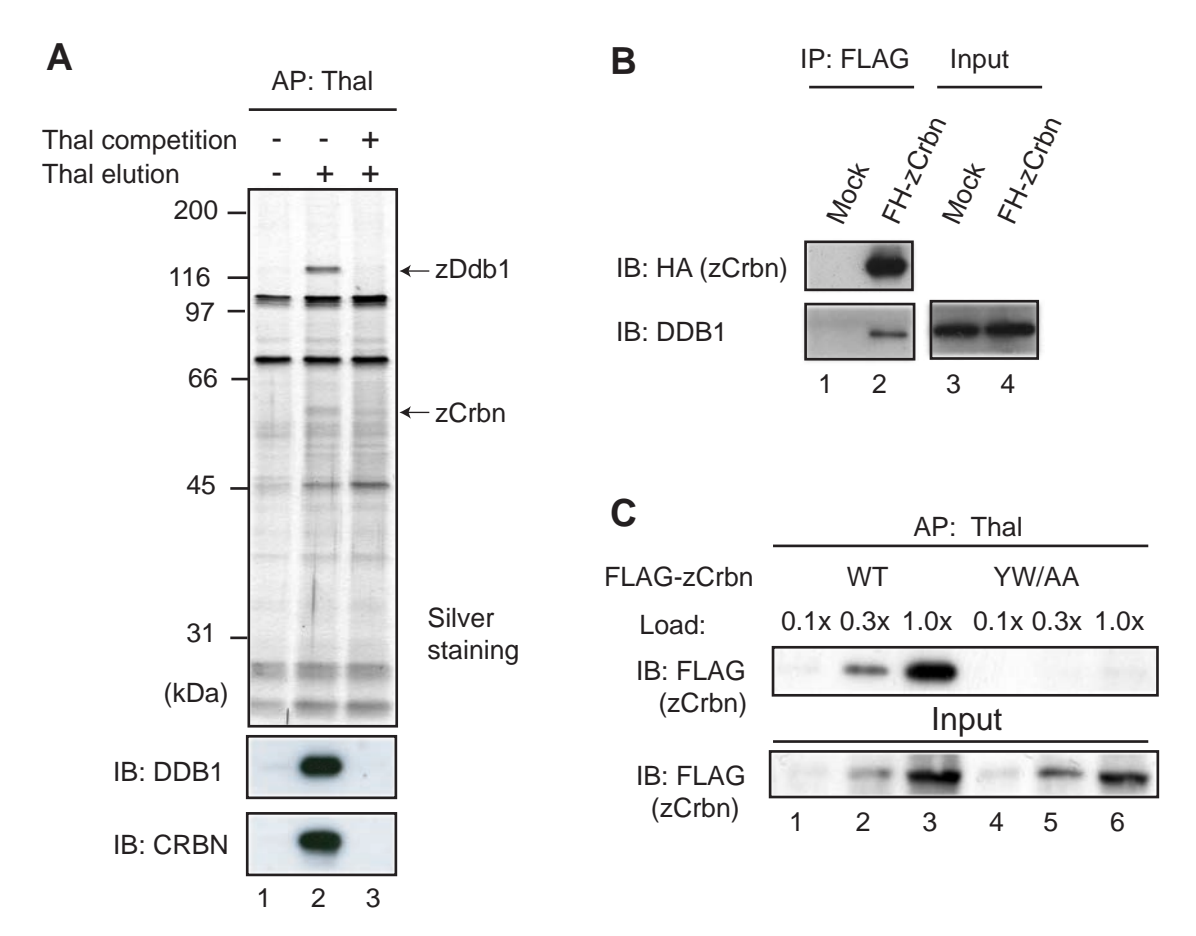
**Fig. S10.** Incidence and spectrum of pectoral fin malformations in zebrafish. (**A**) Diagnostic criteria. The length between the proximal-most end of endoskeletal disc and the distal-most end of actinotrichs was used for classification. Fins that stretched out from the body wall and were more than 85% in length compared to control fins were defined as "no effect." Fins that stretched out but were shortened to 75-85% of control length were defined as "mild" phenotypes. Fins that were attached to the body wall and were shortened to 60 to 75% of control length were defined as "medium" phenotypes. Fins that showed disc-like morphology and were shortened to less than 60% of control length were defined as "severe" phenotypes. (**B** to **E**) Based on the criteria shown in (A), 72-hpf fixed embryos were classified into four groups. (B), (C), and (D) are complementary to the data shown in Fig. 5A, 4C, and 4E, respectively. In (E), thalidomide was added at different time points. uninj, uninjected.



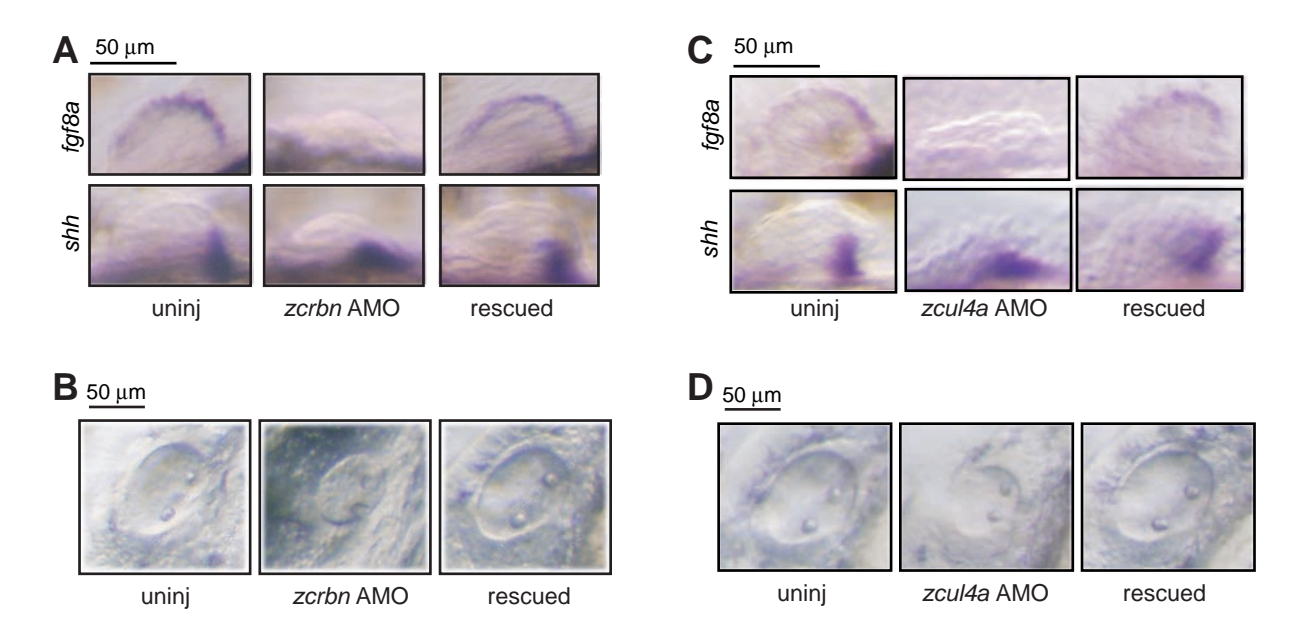
**Fig. S11.** Incidence and spectrum of developmental defects of zebrafish otic vesicles. (**A**) Diagnostic criteria. The major diameter of elliptically-shaped otic vesicles was used for classification. Otic vesicles that were more than 85% in length compared to control were defined as "no effect." Otic vesicles that were reduced to 75-85% of control were defined as "medium" phenotypes. Otic vesicles that were reduced to less than 75% of control were defined as "severe" phenotypes. (**B** to **D**) Based on the criteria shown in (A), 30-hpf fixed embryos were classified into three groups. (B), (C), and (D) are complementary to the data shown in Fig. 5B, 4D, and 4F, respectively. uninj, uninjected.



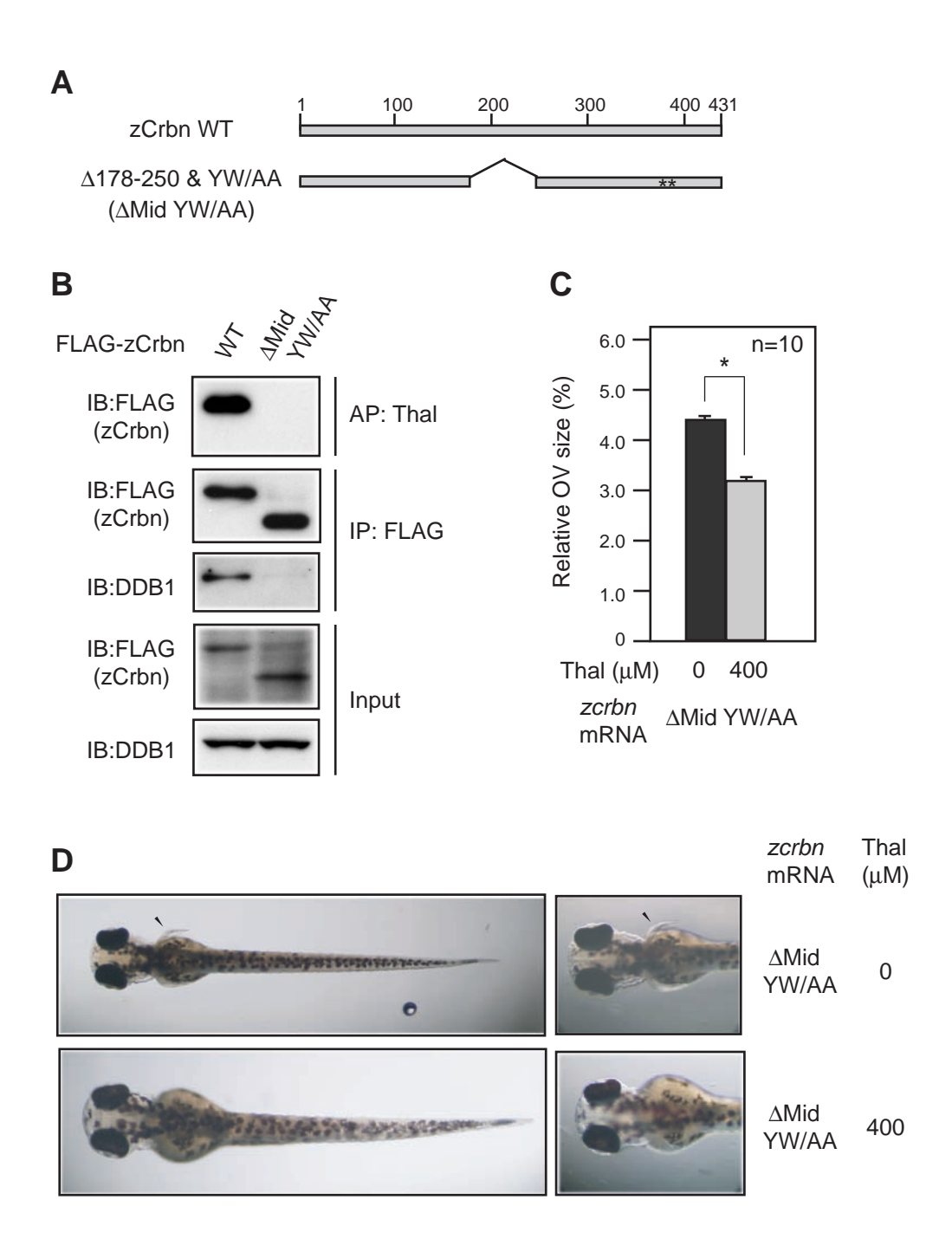
**Fig. S12.** Whole-mount *in situ* hybridization analysis of *zcrbn* and *zcul4a* expression in 30- and 48-hpf zebrafish embryos. (**A** and **B**) *zcrbn* is highly expressed at brain and otic vesicles (OV, arrowheads) at 30 hpf. Lateral (A) and dorsal views (B) are shown. (**C**) *zcul4a* is expressed abundantly at brain at 30 hpf. Lateral view. (**D**) zcrbn is highly expressed at head vasculature (hv), pectoral fin (pf), and brain at 48 hpf. Lateral view. (**E**) *zcrbn* expression at otic vesicles (OV, arrowheads) at 48 hpf. Dorsal view. (**F**) Close-up view of *zcrbn* expression at pectoral fin at 48 hpf. Expression is seen at high levels at proximal mesenchyme (pm) and weakly in migratory mesenchyme (mm). (**G**) *zcul4a* is expressed abundantly at forebrain, midbrain, hindbrain (hb), and pectoral fin (pf) at 48 hpf. Lateral view. (**H**) Expression of *fgf8a* in 48-hpf embryos was examined as a control. *fgf8a* is expressed at mid-hindbrain boundary (MHB) and hindbrain (hb). Lateral view. Anterior is left in all panels except (E) and (F). In (E), anterior is up. Scale bars, 200 μm.



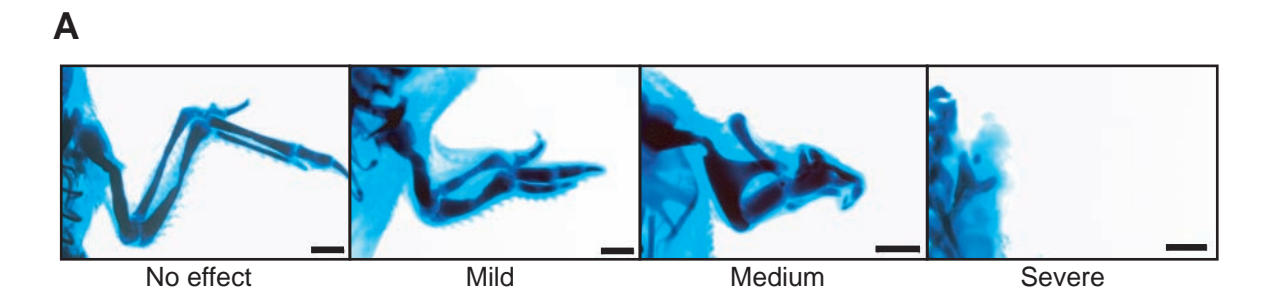
**Fig. S13.** Biochemical analysis of zebrafish Crbn. (**A**) zCrbn binds to thalidomide. Extracts prepared from 30-hpf zebrafish embryos were subjected to affinity purification (AP) with thalidomide (Thal) beads. Eluate fractions were analyzed by silver staining (upper panel) and immunoblotting (IB, bottom panel). (**B**) FH-zCrbn was overexpressed in 293T cells and immunoprecipitated (IP) with anti-FLAG antibody, and coprecipitated endogenous DDB1 was detected by immunoblotting. (**C**) FLAG-zCrbn or FLAG-zCrbn overexpressed in 293T cells was subjected to affinity purification with thalidomide beads. For quantification, various amounts of input and eluate fractions were analyzed by immunoblotting.



**Fig. S14.** Knockdown of *zcrbn* or *zcul4a* causes specific defects in zebrafish fin and otic vesicle development and a reduction of *fgf8a* expression in the AER. (**A** to **D**) Control embryos (uninj), embryos injected with the indicated AMOs, or embryos injected with the AMOs and the corresponding mRNAs (rescued) were examined. In (A) and (C), 48-hpf embryos were subjected to hybridization with antisense probes for *fgf8a* or *shh*. Representative close-up views of fin buds are shown. In (B) and (D), representative close-up views of otic vesicles of 30-hpf live embryos are shown.



**Fig. S15.** zCrbn $^{\Delta Mid\ YW/AA}$ , a zCrbn mutant that does not form an E3 ubiquitin ligase complex, does not suppress thalidomide-induced teratogenicity in zebrafish. (**A**) Schematic structure of zCrbn $^{\Delta Mid\ YW/AA}$ . Asterisk indicates the positions of alanine substitutions. (**B**) zCrbn $^{\Delta Mid\ YW/AA}$  does not bind to DDB1 and thalidomide. Coimmunoprecipitation and affinity purification of FLAG-zCrbn $^{\Delta Mid\ YW/AA}$  were performed as in fig. S13, B and C, respectively. (**C** and **D**) Embryos were injected with zCrbn $^{\Delta Mid\ YW/AA}$  mRNA and were allowed to develop in the presence or absence of thalidomide. (C) Otic vesicle size was measured at 30 hpf and expressed as a ratio to the size of the embryo. \*, p<0.001. (D) Dorsal views of embryos and close-up views of pectoral fins at 72 hpf. Pectral fins are indicated with arrowheads.



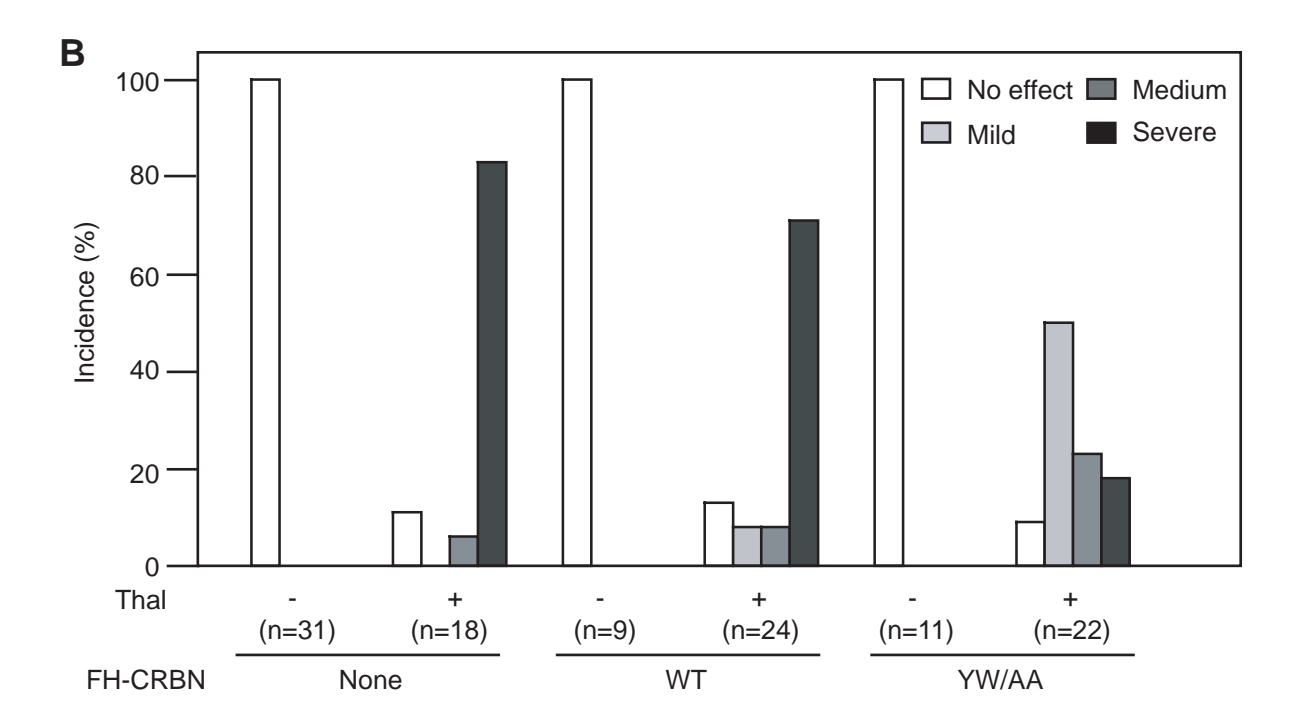


**Fig. S16.** Incidence and spectrum of limb malformations in chick. (**A**) Diagnostic criteria. Scale bar, 1 mm (**B**) At St. 36, skeletal cartilages were stained with Victoria blue, and based on the criteria shown in (A), phenotypes were classified into four groups. These data are complementary to the data shown in Fig. 6.

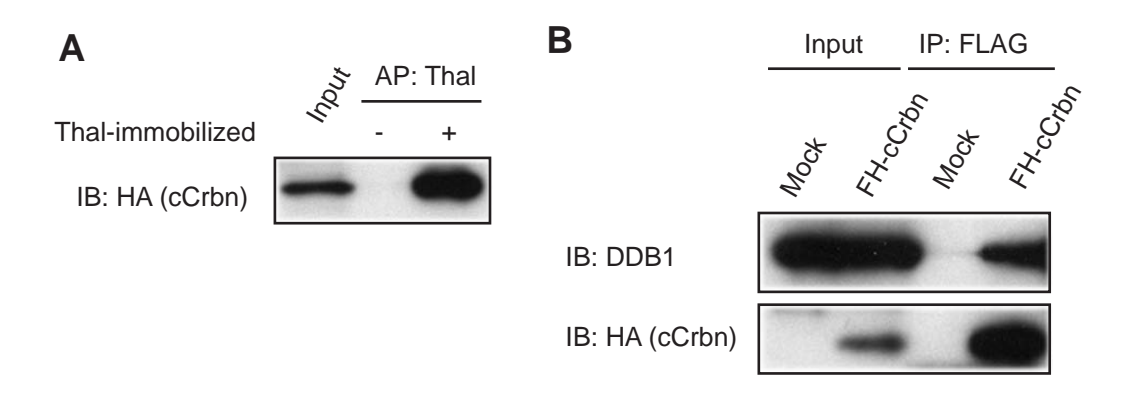


**Fig. S17.** Biochemical analysis of chick Crbn. (**A**) cCrbn binds to thalidomide. FH-cCrbn overexpressed in 293T cells was subjected to affinity purification (AP) with thalidomide (Thal) beads. Lysates (input) and affinity-purified materials were subjected to immunoblotting (IB). (**B**) cCrbn binds to DDB1. FH-cCrbn was overexpressed in 293T cells and immunoprecipitated (IP) with anti-FLAG antibody, and coprecipitated endogenous DDB1 was detected by immunoblotting.

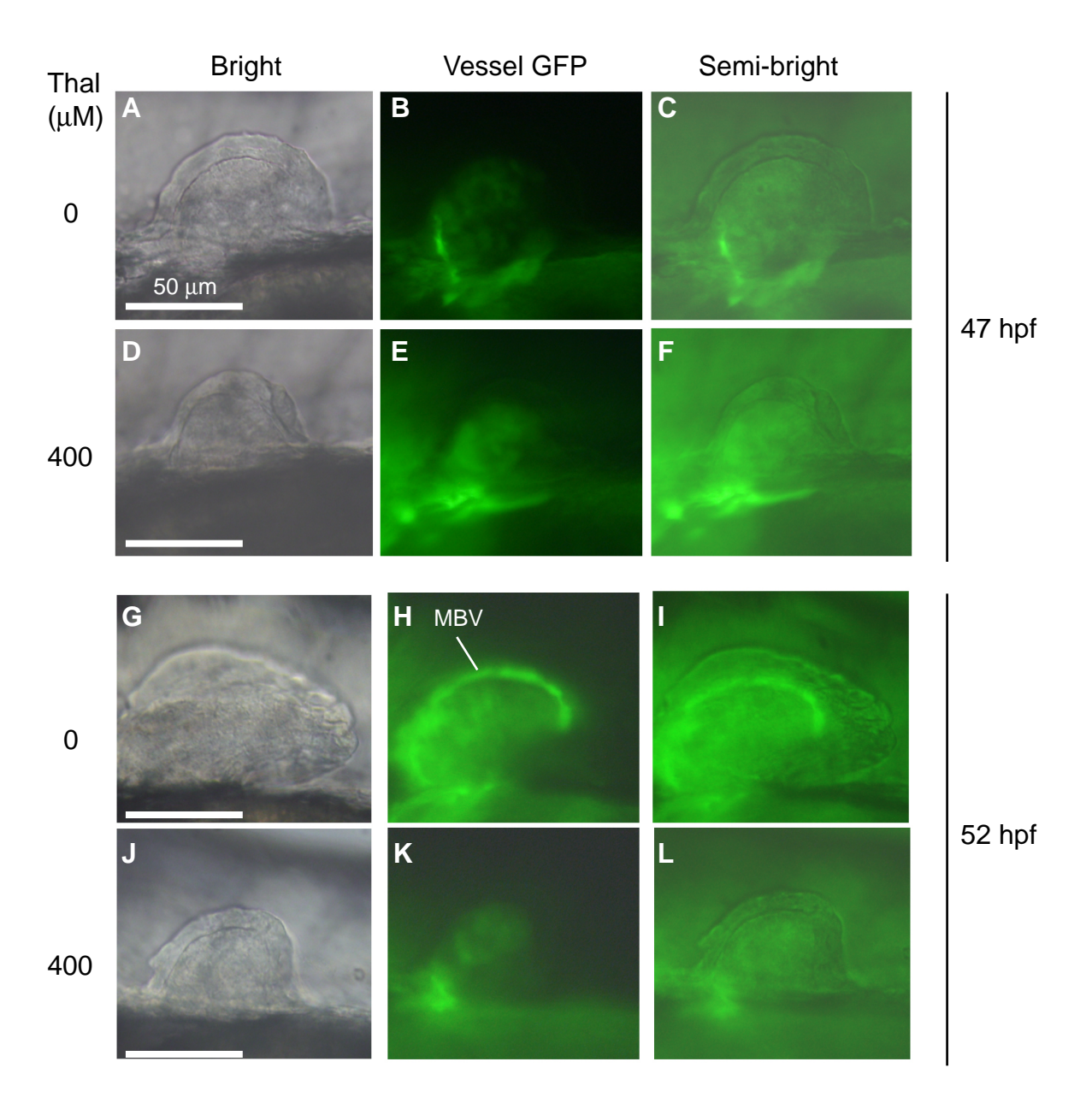


**Fig. S18.** Anti-angiogenic effects of thalidomide on zebrafish pectoral fin buds. fli1a:EGFP transgenic zebrafish embryos were allowed to develop in the presence or absence of thalidomide. (**A-F**) Close-up views of fin buds at 47 hpf. At this stage, the marginal blood vessel (MBV) is not yet formed. (**G-L**) Close-up views of fin buds at 52 hpf. At this stage, The MBV looping around the bud is evident (H). Scale bar,  $50 \, \mu m$ .

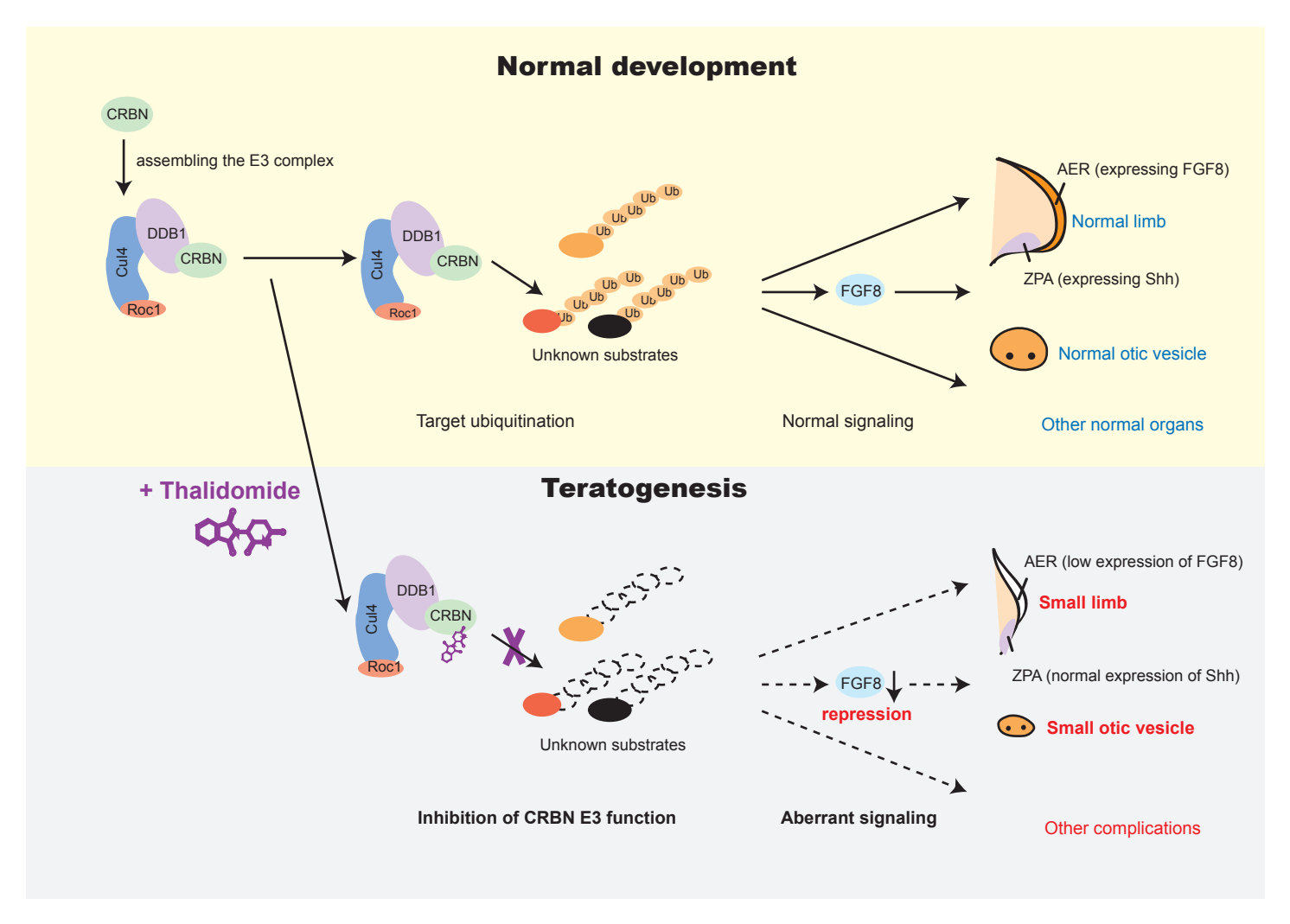


**Fig. S19.** Schematic model for the molecular mechanism of thalidomide teratogenicity. Normally, CRBN functions as a component of the E3 ubiquitin ligase to regulate multiple developmental processes, such as limb and otic vesicle formation, by ubiquitinating unknown substrates (top). Thalidomide binds to CRBN and inhibits the associated E3 function (bottom). Aberrant accumulation of its substrate(s) causes multiple developmental defects, such as small limb and otic vesicle, in part through downregulation of FGF8 expression.

Table S1. Peptide sequences of thalidomide-binding proteins determined by tandem mass spectrometry.

Protein Name	Obtained peptides
Cereblon (CRBN)	VAACLPIDDVLR
	TFAVLAYSNVQER
	WLYSLYDAETLMDR
Damaged DNA binding protein 1 (DDB1)	GESKDLLFILTAK
	ETDDTLVLSFVGQTR
	LICYQEVSQCFGVLSSR,
	SVLLLAYKPMEGNFEEIAR
	IEVQDTSGGTTALRPSASTQALSSSVSSSK

**Table S2.** siRNA knockdown efficiency determined by real-time RT-PCR.

siRNA name	Knockdown efficiency
CRBN #1	95%
CRBN #2	93%
DDB1 #1	94%
DDB1 #2	89%
Cul4A #1	98%
Cul4A #2	98%